A New Interconnecting Layer of Metal Oxide/Dipole Layer/Metal Oxide for Efficient Tandem Organic Solar Cells

Shunmian Lu, Xing Guan, Xinchen Li, Wei E. I. Sha, Fengxian Xie, Hongchao Liu, Jiannong Wang, Fei Huang, and Wallace C. H. Choy**

A new metal-oxide-based interconnecting layer (ICL) structure of all-solution processed metal oxide/dipole layer/metal oxide for efficient tandem organic solar cell (OSC) is demonstrated. The dipole layer modifies the work function (WF) of molybdenum oxide (MoO_x) to eliminate preexisted counter diode between MoO_x and TiO_2. Three different amino functionalized water/alcohol soluble conjugated polymers (WSCPs) are studied to show that the WF tuning of MoO_x is controllable. Importantly, the results show that S-shape current density versus voltage (*J*–*V*) characteristics form when operation temperature decreases. This implies that thermionic emission within the dipole layer plays critical role for helping recombination of electrons and holes. Meanwhile, the insignificant homotandem open-circuit voltage (V_{oc}) loss dependence on dipole layer thickness shows that the quantum tunneling effect is weak for efficient electron and hole recombination. Based on this ICL, poly(3-hexylthiophene) (P3HT)-based homotandem OSC with 1.20 V V_{oc} and 3.29% power conversion efficiency (PCE) is achieved. Furthermore, high efficiency poly(4,8-bis(5-(2-ethylhexyl)-thiophene-2-yl)-benzo[1,2-b54,5-b9]dithiophene-alt alkylcarbonylthieno[3,4-b]thiophene) (PBDTTT-C-T)-based homotandem OSC with 1.54 V V_{oc} and 8.11% PCE is achieved, with almost 15.53% enhancement compared to its single cell. This metal oxide/dipole layer/metal oxide ICL provides a new strategy to develop other qualified ICL with different hole transporting layer and electron transporting layer in tandem OSCs.

1. Introduction

In the past decade, organic solar cells (OSCs) have attracted tremendous attention, thanks to their advantages of low cost, light weight, and mechanical flexibility.[1] Great efforts, such as utilizing plasmonic nanostructure,[2] optimizing device structure,[3] morphology control,[4] developing qualified interface layer,[5] synthesizing novel photoactive polymer, and engineering multijunction (tandem) OSCs,[6,7] have been made to boost its efficiency. Tandem OSCs have the potential to achieve >15% power conversion efficiency (PCE) by fully utilizing the whole solar spectrum and minimizing thermalization loss.[8] A number of high efficiency tandem OSCs with both inverted and normal structures have been reported.[9] Interconnecting layer (ICL) in tandem OSCs, which is important for device efficiency, shall meet the following requirements: (1) electrically, the ICL should form equivalent ohmic contact so that the addition of V_{oc} has no loss; (2) optically, it should have transparency as high as possible; and (3) at the same time, ICL should provide robust platform for forming top cell without dissolving the bottom cell due to solvent penetration. These three requirements make ICL one of the most challenging issues in tandem OSCs.

The combination of different electron transport layer (ETL) and hole transport layer (HTL) has been reported for ICL in tandem solar cell.[10] The typical ETLs in OSCs include transparent transition metal oxides, such as titanium dioxide (TiO_2),[3a,11] zinc oxide (ZnO),[12] and polymer dipole layers, such as poly[(9,9-bis(3′-(*N*,*N*-dimethylamino)propyl)-2,7-fluorene)-alt-2,7-(9,9-dioctylfluorene)] (PFN),[13] ethoxylated polyethylenimine (PEIE).[14] For HTL, transparent metal oxides such as vanadium oxide (V_2O_5),[15] molybdenum trioxide (MoO_3),[15b,d,16] nickel oxide (NiO_x),[17] and conductive polymers, such as poly(3,4-ethylenedioxythiophene):poly(styrenesulfonate) (PEDOT:PSS),[18] are widely adopted in OSCs. Nonetheless, the appropriate selections of those ETL and HTL are critical to reduce V_{oc} loss in tandem OSCs due to the quasi-Fermi level difference in the ICL. There are two strategies to overcome this counter diode issue in ICL. One is to form tunneling junction in ICL by using heavily doped ETL and heavily doped HTL. The combination of PEDOT:PSS (a heavily doped HTL) and TiO_2/ZnO

S. Lu, X. Li, Dr. W. E. I. Sha, Dr. F. Xie, Prof. W. C. H. Choy
Department of Electrical and Electronic Engineering
The University of Hong Kong
Pokfulam Road, Hong Kong, China
E-mail: chchoy@eee.hku.hk

X. Guan, Prof. F. Huang
Institute of Polymer Optoelectronic Materials and Devices
State Key Laboratory of Luminescent Materials and Devices
South China University of Technology
Guangzhou 510640, P. R. China
E-mail: msfhuang@scut.edu.cn

H. Liu, Prof. J. Wang
Department of Physics
The Hong Kong University of Science and Technology
Clear Water Bay, Kowloon, Hong Kong

DOI: 10.1002/aenm.201500631

(a heavily doped ETL after UV activation) has been reported as qualified ICL in OSCs.[7c,9d,19] However, typically, the acidic and hygroscopic characteristics of PEDOT:PSS have been largely criticized for decrementing the device stability and UV excitation for TiO_2/ZnO is required to remove the S-shape in tandem *J–V* characteristics.[20] The other commonly used strategy to overcome the counter diode issue in ICL is to form a very thin layer of metal or metal nanoclusters between the HTL and ETL to better align the quasi-Fermi level. In this case, metal oxide HTL and ETL, such as MoO_3 and TiO_2/ZnO, are used as part of ICL, between which Ag, Al, or Au nanoclusters, thermally evaporated under high vacuum condition, act as recombination center to better align metal oxides quasi-Fermi level.[10a,21] However, this metal oxide/metal/metal oxide ICL usually results in some small amount of V_{oc}, J_{sc}, and fill factor (FF) loss due to incomplete separation of ETL and HTL, decreased ICL optical transmittance and high series resistance, respectively. Simple solution process for the whole ICL structure with the features of water-free, pH neutral, and no counter diode formation is highly desirable for the evolution of tandem OSCs.

In this work, we propose a new metal oxide/dipole layer/metal oxide ICL structure for tandem OSCs, which provides a new strategy to combine different ETL and HTL as qualified ICL. With the proper choose of dipole layer, our results show that the counter diode between MoO_x and TiO_2 has been successfully eliminated, resulting in no V_{oc} loss in tandem structure. In addition, our structure formed from MoO_x, dipole material, and TiO_2 has the interesting features of water free, all-solution, room atmosphere, and low-temperature process, which are suitable for large area solution processes such as roll-to-roll printing, spray and spin coating. Meanwhile, the processing temperature of the ICL is under 100 °C, which is of great benefit for deposition of photoactive layer to avoid high temperature detriments. Interestingly, temperature sensitive thermionic emission mechanism rather than the thickness sensitive quantum tunneling contributes to the carrier recombination through ICL in the tandem OSC. Our results based on this all-solution processed metal oxide/dipole layer/metal oxide ICL show very good current density versus voltage (*J–V*) characteristics. We demonstrate a 1.20 V V_{oc} and 3.29% PCE tandem OSC consisting of two identical subcells (homo-tandem) from poly(3-hexylthiophene) (P3HT) and [6,6]-phenyl C61-butyric acid methylester ($PC_{60}BM$). By replacing P3HT:$PC_{60}BM$ with low bandgap material of poly(4,8-bis(5-(2-ethylhexyl)-thiophene-2-yl)-benzo[1,2-b54,5-b9]dithiophene-alt alkylcarbonylthieno[3,4-b]thiophene) (PBDTTT-C-T):[6,6]-phenyl C71-butyric acid methyl ester ($PC_{70}BM$), we demonstrate 8.11% PCE with 1.54 V V_{oc} in its homo-tandem structure, which is almost 15.53% enhancement from its single cell. As a result, this metal oxide/dipole layer/metal oxide ICL structure provides a new strategy for developing other qualified ICL in tandem OSCs.

2. Results and Discussion

2.1. Electrical and Optical Properties of MoO_x/Dipole Layer/TiO_2 ICL

The studied device structure is indium tin oxide (ITO)/TiO_2/P3HT:$PC_{60}BM$/MoO_x/dipole layer/TiO_2/P3HT:$PC_{60}BM$ /MoO_x/Ag as shown in **Figure 1**a. The ICL is MoO_x/dipole layer/TiO_2, which is all-solution processed. The synthesis route of the MoO_x solution was outlined in previous reports.[15b,16b] The TiO_2 nanoparticles was synthesized by a nonaqueous method.[22] The dipole layer is amino functionalized water/alcohol soluble conjugated polymers (WSCPs) including poly[(2,7-(9,9-bis(6-(*N*,*N*-diethylamino)-hexyl)fluorene))-alt-(2,5-pyridinyl)] (PF6N25Py), poly[(2,7-(9,9-bis(6-(*N*,*N*-diethylamino)-hexyl *N*-oxide)fluorene))-alt-(2,6-pyridinyl)](PF6NO26Py) and poly[(2,7-(9,9-bis(6-(*N*,*N*-diethylamino)-hexyl *N*-oxide)fluorene))-alt-(3,5-pyridinyl)] (PF6NO35Py), the chemical structure of which is shown in Figure S1 (Supporting Information).[23] PF6N25Py shows the best characteristics in our MoO_x/dipole layer/TiO_2 tandem structure as will be discussed later. Details of the device fabrication are described in the Experimental Section.

The work function (WF) of the WSCPs on MoO_x film is measured by Kevin probe in air as shown in **Table 1**. The pristine MoO_x has 5.42 eV WF, which is suitable for efficient HTL in OSCs. With the deposition of PF6NO26Py, PF6NO35Py, and PF6N25Py dipole layer, the WF of MoO_x is modified significantly from 5.42 to 4.71, 4.43, and 4.18 eV, respectively. The dipole layer can therefore diminish or even eliminate the counter diode effects between MoO_x with 5.42 eV WF and TiO_2 with 4.20 eV WF. By inserting the above three dipole layers between MoO_x and TiO_2, homo-tandem OSCs with the structure of ITO/TiO_2/P3HT:$PC_{60}BM$/MoO_x/dipole layer/TiO_2/P3HT:$PC_{60}BM$/MoO_x/Ag have been fabricated to study the counter diode effect in the ICL. The photovoltaic parameters (including V_{oc}, J_{sc}, FF, and PCE) and *J–V* characteristics are shown in Table 1 and Figure 1d, respectively. For MoO_x direct contacting with TiO_2 (Device A), the homo-tandem OSC has 0.81 V V_{oc}, 2.11 mA cm^{-2} J_{sc}, 42.18% FF, and 0.72% PCE. For the ICL with PF6N25Py inserted between MoO_x and TiO_2 (Device D), it shows 1.20 V V_{oc}, 4.31 mA cm^{-2} J_{sc}, 63.83% FF, and 3.29% PCE. The V_{oc} loss of about 0.40 V from Device A is from the formation of counter diode between MoO_x with 5.42 eV WF and TiO_2 with 4.20 eV WF. This counter diode introduces a barrier for holes from the first subcell through MoO_x to recombine with electrons from the second subcell through TiO_2. Besides V_{oc} loss, Device A's J_{sc} has been largely limited and FF has been greatly decreased compared to Device D. Device B (Device C) with PF6NO26Py (PF6NO35Py) inserted between MoO_x and TiO_2 in the P3HT:$PC_{60}BM$ homo-tandem OSC shows 0.95 V V_{oc}, 3.38 mA cm^{-2} J_{sc}, 51.24% FF, 1.65% PCE (1.10 V V_{oc}, 3.86 mA cm^{-2} J_{sc}, 53.31% FF, and 2.26% PCE). The results indicate the smaller the counter diode barrier formed between MoO_x and TiO_2, the better the V_{oc}, J_{sc}, FF, and PCE of P3HT:$PC_{60}BM$ homo-tandem OSCs. The band diagram of P3HT:$PC_{60}BM$ homo-tandem OSCs based on MoO_x/PF6N25Py/TiO_2 ICL is shown in Figure 1c featured in a dipole between MoO_x/TiO_2 to eliminate its otherwise existed counter diode. In addition, the ICL solvent protection of bottom cell from dissolving by top cell is illustrated from scanning electron microscope (SEM) image of the well-defined individual layers of the homo-tandem OSCs as shown in Figure 1b. The thickness of ITO is about 100 nm. The first and second P3HT:$PC_{60}BM$ layers are about 50 nm, the TiO_2 about 40 nm, and the ICL about 50 nm. The MoO_x/PF6N25Py/TiO_2 ICL can be observed although individual layer is too thin to be resolved in the SEM.

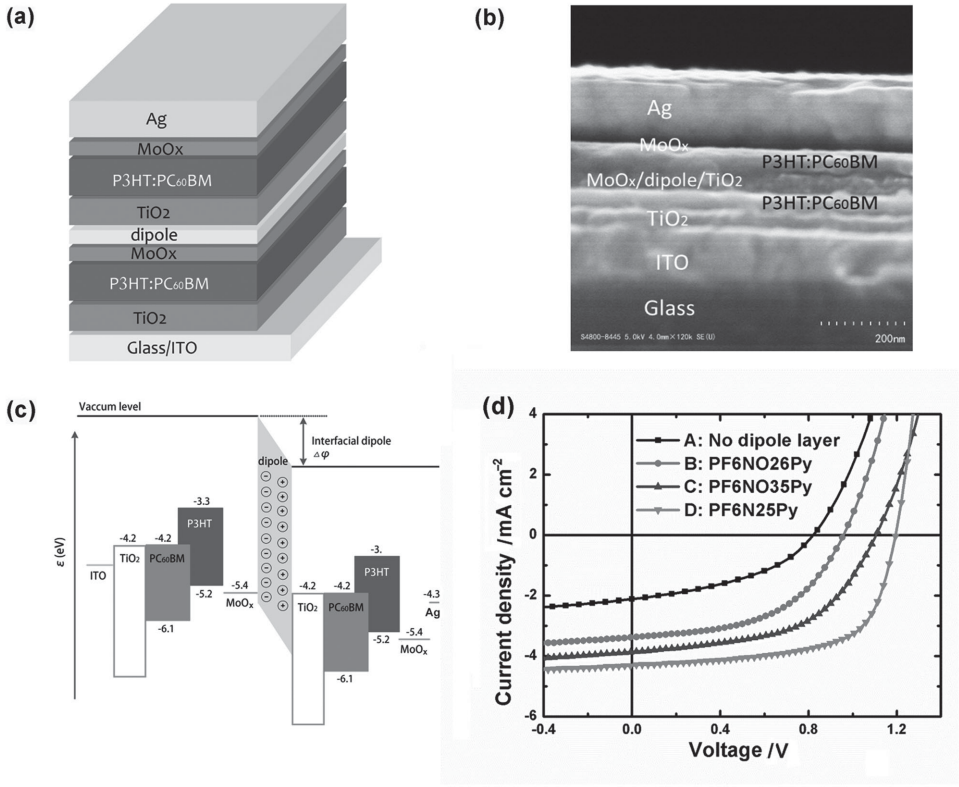

Figure 1. Homo-tandem OSCs based on MoO_x/dipole layer/TiO_2 ICL. a) The device structure. b) The SEM cross section. c) The band diagram. d) The *J*–*V* characteristics.

The thickness of each components of ICL is measured by ellipsometry with MoO_x as 8.1 nm, dipole layer as 6.2 nm, and TiO_2 as 40.3 nm. Consequently, the dipole layer provides controllable WF tuning of MoO_x and good film protection for tandem OSCs.

To reconfirm that the new MoO_x/PF6N25Py/TiO_2 works as qualified ICL, a series of single OSCs with structures shown as Devices E, F, and G have been fabricated and investigated. The efficient combination of metal oxide/dipole layer/metal oxide working as equivalent ohmic contact shall show the same functionality as the commonly used single ETL layer (TiO_2) in inverted single-junction devices.[20a]

Device E: ITO/TiO_2/P3HT:PC_{60}BM/MoO_x/Ag
Device F: ITO/MoO_x/TiO_2/P3HT:PC_{60}BM/MoO_x/Ag
Device G: ITO/MoO_x/PF6N25Py/TiO_2/P3HT:PC_{60}BM/ MoO_x/Ag

The photovoltaic parameters and *J*–*V* characteristics are shown in Table S1 and Figure S2 (Supporting Information), respectively. Device E is the control device with an inverted single P3HT:PC_{60}BM structure based on TiO_2 as single ETL, which shows a good performance of 0.60 V V_{oc}, 9.44 mA cm^{-2} J_{sc}, 64.48% FF, and 3.65% PCE. For MoO_x/TiO_2 without PF6N25Py to serve as ETL shown in Device F, J_{sc}, and V_{oc} decrease dramatically due to the formation of inverse p–n junction, where the extraction of electrons from TiO_2 to ITO is largely limited by the Schottky electron barrier at MoO_x/TiO_2 interface. The introduction of PF6N25Py dipole layer in Device G generates an appropriate dipole between MoO_x and TiO_2. Consequently, the equivalent ohmic contact in MoO_x/PF6N25Py/TiO_2 of Device G shows a comparable *J*–*V* characteristics (0.59 V V_{oc}, 9.78 mA cm^{-2} J_{sc}, 62.31% FF, and 3.60% PCE) to Device E.

To understand the electron and hole recombination mechanism of the new ICL of MoO_x/PF6N25Py/TiO_2, a series of temperature-dependent *J*–*V* characteristics have been measured based on MoO_x/PF6N25Py/TiO_2 and MoO_x/TiO_2 ICL,

Table 1. Photovoltaic parameters of P3HT:PC_{60}BM homo-tandem OSCs based on different dipole layers inserted between MoO_x and TiO_2.

Device no.	Dipole layer	J_{sc} [mA cm^{-2}]	V_{oc} [V]	FF [%]	PCE [%]	Part of ICL layer	Kevin probe WF [eV]
Device A	No dipole layer	2.11	0.81	42.18	0.72	MoO_x	5.42 ± 0.05
Device B	PF6NO26Py	3.38	0.95	51.24	1.65	MoO_x/PF6NO26Py	4.71 ± 0.06
Device C	PF6NO35Py	3.86	1.10	53.31	2.26	MoO_x/PF6NO35Py	4.33 ± 0.06
Device D	PF6N25Py	4.31	1.20	63.38	3.29	MoO_x/PF6N25Py	4.18 ± 0.05

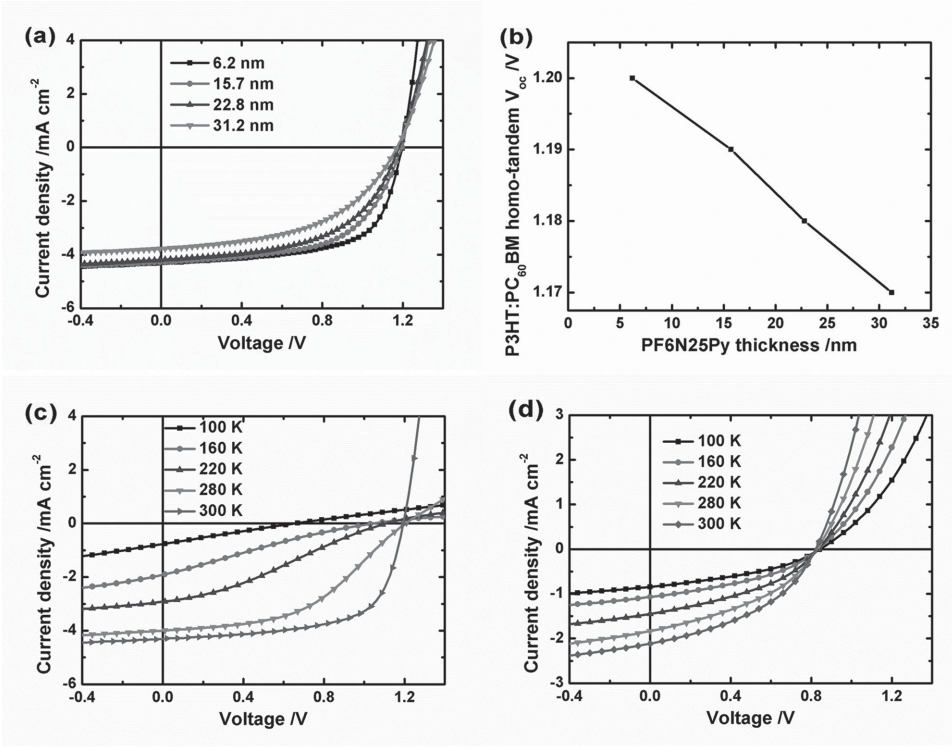

Figure 2. a) *J–V* characteristics of P3HT:PC_{60}BM homo-tandem OSCs with different thicknesses of PF6N25Py in MoO_x/dipole layer/TiO_2 ICL. b) V_{oc} dependence on different thicknesses of PF6N25Py in MoO_x/dipole layer/TiO_2 ICL. c) The temperature-dependent *J–V* characteristics of P3HT:PC_{60}BM homo-tandem OSCs based on MoO_x/PF6N25Py/TiO_2 ICL and d) MoO_x/TiO_2 ICL.

respectively, as shown in **Figure 2**. For P3HT:PC_{60}BM homo-tandem OSCs based on MoO_x/TiO_2 ICL, it is shown that the V_{oc} remains almost unchanged while J_{sc} suffers reduction when temperature decreases from 300 to 100 K. As a comparison, the *J–V* characteristics of P3HT:PC_{60}BM homo-tandem OSCs based on MoO_x/PF6N25Py/TiO_2 ICL show a distinctive s-shape when temperature is decreased from 300 K. At the same time, both J_{sc} and V_{oc} drop gradually when temperature reduces from 300 to 280, 220, 160, and 100 K. We can understand the results as thermionic emission within PF6N25Py for helping electrons and holes to recombine. When the temperature decreases, a barrier for holes from MoO_x of first cell and electrons from the TiO_x of the second cell appears, hindering the efficient carrier recombination via dipole layer in the ICL and resulting in S-shape *J–V* characteristics. To further investigate the electron and hole recombination mechanism in the ICL, a series of P3HT:PC_{60}BM homo-tandem OSCs with different thickness of PF6N25Py have been fabricated and their *J–V* characteristics and photovoltaic parameters are shown in Figure 2a and Table S2 (Supporting Information), respectively. As the thickness of PF6N25Py increases from 6.2 to 15.7, 22.8, and 31.2 nm (measured by ellipsometry), the V_{oc} of P3HT:PC_{60}BM homo-tandem OSCs remains almost unchanged with tiny loss up to 0.03 V. The linear dependence of V_{oc} on PF6N25Py thickness as shown in Figure 2b confirms that the tunneling effect in MoO_x/PF6N25Py/TiO_2 ICL is weak for the recombination of carriers in the ICL.[24] The tiny V_{oc} loss can be explained by the induced series resistance voltage loss of PF6N25Py. Consequently, the electrical role of PF6N25Py lies mainly in two aspects: (1) exerting a dipole to form ohmic contact for electrons from the top subcell travelling towards ICL to recombine with the holes from the bottom subcell and (2) thermionic emission mechanism rather than the tunneling within PF6N25Py is accounted for the carrier recombination in the ICL.

The optical transmission of MoO_x/PF6N25Py/TiO_2 ICL shows a very high transparency covering the wavelength from 350 to 1000 nm as shown in Figure S3 (Supporting Information). There is a small peak of 82% at the wavelength of 350 nm and a valley of 77% at the wavelength of 410 nm, which is mainly due to the 400 nm absorption peak of PF6N25Py.[23] At the wavelength of 410 nm, the transmission increases rapidly and finally reaches an average close to 95% between 480 and 1000 nm. This high transparency is highly desirable in ICL to minimize absorption loss.

2.2. Optimized P3HT:PC_{60}BM Homo-Tandem OSCs

Homo-tandem organic solar cell has been reported as a prototype for organic tandem structure, which can boost its single device's efficiency due to enhanced absorption and charge extraction simultaneously.[25] Theoretically for organic solar cell, if one increases the film thickness to get higher J_{sc}, the PCE is limited by the lower FF due to inferior carrier mobility induced recombination loss. In order to get optically thick and electrically thin device structure to both enhance light absorption and charge extraction, it is feasible to split a thick film single junction into two thin subcells in tandem.

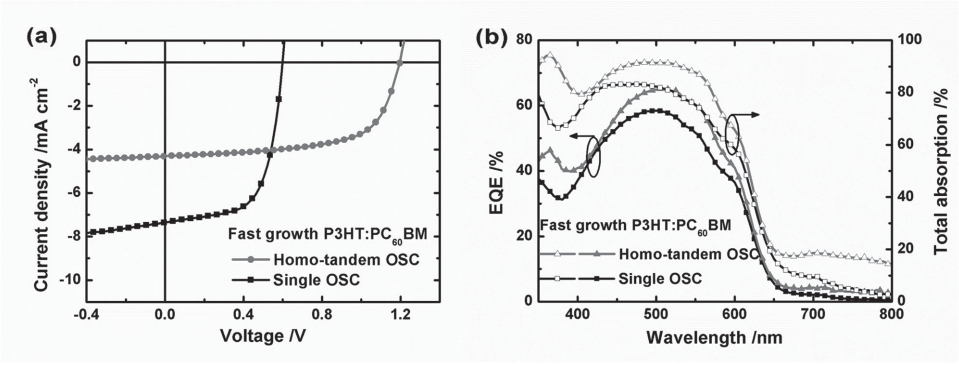

Figure 3. Fast growth single and homo-tandem P3HT:PC_{60}BM OSCs: a) *J–V* characteristics and b) absorption and EQE.

An optimized P3HT:PC_{60}BM homo-tandem OSC based on this new ICL has achieved 3.29% PCE, which demonstrates the MoO_x/dipole layer/TiO_2 as a qualified ICL in tandem OSCs. The optimized thickness of first and second cell of P3HT:PC_{60}BM are about 50 nm and the optimized thickness of PF6N25Py dipole layer is about 6.2 nm. Their *J–V* characteristics and photovoltaic parameters are shown in **Figure 3**a and **Table 2**, respectively. For total V_{oc}, this ICL shows doubled 1.20 V V_{oc} without voltage loss. In P3HT:PC_{60}BM homo-tandem OSC, to balance the photon absorption in its subcells, thin first and second photoactive layers have been formed by fast spin-coating velocity without slow growth process. Thus for an objective comparison of J_{sc} enhancement, a fast growth single P3HT:PC_{60}BM OSC has been optimized as control device, which has 0.60 V V_{oc}, 7.36 mA cm^{-2} J_{sc}, 63.34% FF, and 2.80% PCE. It can be observed that the sum J_{sc} of the two subcells in P3HT:PC_{60}BM homo-tandem OSC is 8.62 mA cm^{-2}, which is 17.11% enhancement compared to optimized fast growth single P3HT:PC_{60}BM OSC. In addition, P3HT:PC_{60}BM homo-tandem OSC shows a slightly higher FF (63.83%) than the corresponding optimized single OSC (63.34%), which is mainly due to the stronger carrier extraction in thinner photoactive layer. As a result, the combined improvement of J_{sc} and FF in P3HT:PC_{60}BM homo-tandem OSC compared to its single OSC yields 17.50% PCE enhancement from 2.80% to 3.29%.

The total absorption of P3HT:PC_{60}BM single and homo-tandem OSCs are shown in Figure 3b. The major absorption enhancement of P3HT:PC_{60}BM homo-tandem OSC covers the wavelength ranging from 350 to 400 and 450 to 600 nm. In terms of external quantum efficiency (EQE), for homo-tandem OSC, measuring its real EQE by light biasing is not practical since it consists identical photoactive layers as its subcells. Thus a calculated measurement is used assuming that the subcells of homo-tandem OSC have the same internal quantum efficiency as its single OSC.[25] The EQE of measured single OSC and calculated homo-tandem OSC EQE are shown in Figure 3b. P3HT:PC_{60}BM homo-tandem OSC shows almost identical EQE to single OSC above 600 nm. For wavelength shorter than 600 nm, especially from 350 to 400 and 450 to 600 nm, an obvious EQE enhancement, which is mainly due to the increased photon absorption, is achieved in P3HT:PC_{60}BM homo-tandem OSC compared to its single OSC.

Table 2. Photovoltaic parameters of fast growth single and homo-tandem P3HT:PC_{60}BM OSCs.

Device no.	P3HT:PC_{60}BM	J_{sc} [mA cm^{-2}]	V_{oc} [V]	FF [%]	PCE [%]
Device H	Fast growth single OSC	7.36	0.60	63.34	2.80
Device I	Fast growth homo-tandem OSC	4.31	1.20	63.83	3.29

In addition, the device characteristics based on evaporated Ag and Al as recombination center between MoO_x and TiO_2 has also been investigated as comparison to our MoO_x/dipole layer/TiO_2 ICL. The Ag and Al thin films with each thickness of 2 nm have been deposited from thermal evaporation on top of solution processed MoO_x. Ag has good contact with MoO_x and thus has been first evaporated on top of MoO_x. However, TiO_2 solution shows high contact angle on top of Ag. In order to solve this issue, another thin layer of Al has been evaporated on top of Ag to increase wetting for further spin coating of TiO_2. The thickness of Ag and Al has been optimized to avoid lateral shorting and maximize transmission. Their *J–V* characteristics and photovoltaic parameters are shown in Figure S4 and Table S3 (Supporting Information), respectively. P3HT:PC_{60}BM homo-tandem OSC based on MoO_x/Ag/Al/TiO_2 ICL shows photovoltaic parameters of 3.39 mA cm^{-2} J_{sc}, 1.16 V V_{oc}, 53.32% FF, and 2.10% PCE. The lower V_{oc} is resulted from the incomplete film separation of MoO_x from TiO_2 since Ag/Al with 2 nm thickness is likely to be nanoclusters rather than continuous thin film. This also introduced a lower FF due to higher R_s (5.18 Ω cm^2 of Deivce M compared to 3.97 Ω cm^2 of Device N) and a lower R_{sh} (1.91 kΩ cm^2 of Device M compared to 3.52 kΩ cm^2 of Device N). The lower J_{sc} is mainly resulted from the transmittance loss in Ag/Al nanoclusters. As a comparison, P3HT:PC_{60}BM homo-tandem OSC based on MoO_x/dipole layer/TiO_2 ICL shows a superior performance to that based on MoO_x/Ag/Al/TiO_2 ICL, resulting in almost 56.67% PCE enhancement from 2.10% to 3.29%.

2.3. High Efficiency PBDTTT-C-T:PC_{70}BM Homo-Tandem OSCs

PBDTTT-C-T:PC_{70}BM homo-tandem OSC has been used to demonstrate our ICL for high efficiency tandem solar cell. The optimized thickness of single PBDTTT-C-T is around 100 nm with device characteristics of 0.77 V V_{oc}, 14.44 mA cm^{-2} J_{sc},

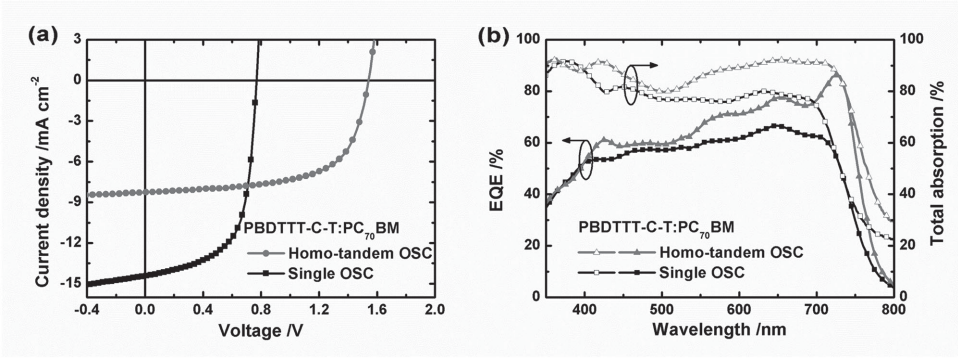

Figure 4. Single and homo-tandem PBDTTT-C-T:$PC_{70}BM$ OSCs: a) *J–V* characteristics and b) absorption and EQE.

63.14% FF, and 7.02% PCE. To balance the current of two subcells in the homo-tandem OSC, the optimized first cell thickness of about 80 nm and second cell of about 90 nm have been fabricated in the homo-tandem OSC. An optimized characteristics of PBDTTT-C-T:$PC_{70}BM$ homo-tandem OSC with 1.54 V V_{oc}, 8.27 mA cm^{-2} J_{sc}, 63.69% FF, and 8.11% PCE has been achieved. Their *J–V* characteristics and photovoltaic parameters are shown in **Figure 4**a and **Table 3**, respectively. The PCE enhancement of PBDTTT-C-T:$PC_{70}BM$ homo-tandem OSC is mainly due to the increased J_{sc} from enhanced absorption. It can be seen in Figure 4b that the absorption enhancement of homo-tandem OSC compared to single OSC is mainly between 400 and 800 nm. Based on the EQE of single PBDTTT-C-T:$PC_{70}BM$ OSC and the absorption of single and homo-tandem OSCs, the EQE of PBDTTT-C-T:$PC_{70}BM$ homo-tandem OSC has been calculated as a reference to its true EQE as shown in Figure 4b. The EQE of PBDTTT-C-T:$PC_{70}BM$ homo-tandem OSC is enhanced almost over the whole absorption spectrum (especially from 550 to 750 nm) compared to its single OSC. The increased J_{sc} and FF with doubled V_{oc} in PBDTTT-C-T:$PC_{70}BM$ homo-tandem OSC yield 15.53% PCE enhancement from 7.02% to 8.11%.

3. Conclusion

In conclusion, a water-free, all-solution, and low temperature processed metal oxide/dipole layer/metal oxide ICL structure, which shows qualified electrical, optical, and protective properties in tandem OSCs structure, has been proposed and demonstrated. This new ICL utilizes dipole layer to modify the work function of MoO_x to eliminate otherwise existing counter diode between MoO_x and TiO_2 in tandem ICL. With WSCPs, we show that WF tuning is controllable by exerting a dipole to form ohmic contact for electrons from the top subcell travelling towards ICL to recombine with the holes from the bottom subcell. Importantly, the electron and hole recombination in the metal oxide/dipole layer/metal oxide ICL can be explained by thermionic emission within dipole layer rather than tunneling process. Based on that, homo-tandem OSCs with doubled V_{oc} and enhanced total J_{sc} have been achieved. A 1.20 V V_{oc} and 3.29% PCE (17.50% enhancement compared to its single OSC) of P3HT:$PC_{60}BM$ homo-tandem OSC and 1.54 V V_{oc} and 8.11% PCE (15.53% enhancement compared to its single OSC) of PBDTTT-C-T:$PC_{70}BM$ homo-tandem OSC have been realized. Consequently, this metal oxide/dipole layer/metal oxide ICL provides a new general strategy to develop other qualified ICL with different HTL and ETL in tandem OSCs.

Table 3. Photovoltaic parameters of single and homo-tandem PBDTTT-C-T:$PC_{70}BM$ OSCs.

Device no.	PBDTTT-C-T:$PC_{70}BM$	J_{sc} [mA cm^{-2}]	V_{oc} [V]	FF [%]	PCE [%]
Device J	Single OSC	14.44	0.77	63.14	7.02
Device K	Homo-tandem OSC	8.27	1.54	63.69	8.11

4. Experimental Section

Material Synthesis and Preparation: Molybdenum powder was purchased from Aladdin Industrial Inc. The MoO_x film is formed from molybdenum bronze solution synthesized by the method described in previous report.[15b,d,16b] The titanium oxide nanoparticle was synthesized by a nonaqueous method dissolved in methanol.[22] A series of amino functionalized water/alcohol soluble conjugated polymers were provided by Huang's group.[23] P3HT, $PC_{60}BM$, and PBDTTT-C-T were purchased from Solarmer Energy, Inc. $PC_{70}BM$ was purchased from Nano-C, Inc.

Fabrication of Single Junction OSCs: ITO glass with a sheet resistivity of 15 Ω square^{-1} was cleaned with detergent, acetone, and ethanol in sequence followed by 15 min UV-ozone treatment. After that, a thin layer of TiO_2 in methanol was spin-casted at 6000 r.p.m. for 40 s and then annealed at 150 °C for 10 min. P3HT:$PC_{60}BM$ (1:1) in 1,2-dichlorobenzene (DCB) with a concentration of 20 mg mL^{-1} was spin coated at 670 r.p.m. for 40 s followed by 1 h slow growth within a petri dish. The samples were then postannealed at 100 °C for 10 min. For fast growth, P3HT:$PC_{60}BM$ with the same concentration in DCB was spin coated at different speed and annealed at 100 °C for 10 min immediately. Regarding OSCs with low bandgap material as active layer, PBDTTT-C-T:$PC_{70}BM$ (1:1.8) in chlorobenzene (CB) with a concentration of 10 mg mL^{-1} and a 3% volume ratio of 1,8-diiodooctane was spin coated at 1500 r.p.m. for 40 s followed by 1 h vacuum treatment. After the deposition of photoactive layer, molybdenum bronze solution was spin coated at 3000 r.p.m. for 30 s before thermal evaporation of 100 nm Ag to complete the device.

Fabrication of Tandem OSCs: For P3HT:$PC_{60}BM$ homo-tandem OSC, P3HT:$PC_{60}BM$ in DCB was spin coated at 2500 r.p.m. for 40 s followed by 100 °C postannealing for 10 min. Molybdenum bronze solution was then spin coated at 3000 r.p.m. for 30 s on top of photoactive layer. Then dipole layer, dissolved in methanol (concentration, 2 mg mL^{-1}) and a small amount of acetic acid (2 μL mL^{-1}), was spin coated above the photoactive layer. A 40 nm TiO_2 layer was spin coated atop. The sample

was annealed at 100 °C for 10 min to form the ICL. Then P3HT:$PC_{60}BM$ in DCB was spin coated at 3000 r.p.m. on top of ICL followed by 100 °C annealing for 10 min. The device was finalized by spin coating a thin layer from molybdenum bronze solution and thermal evaporation of 100 nm Ag. For low bandgap homo-tandem OSC, PBDTTT-C-T:$PC_{70}BM$ dissolving in chlorobenzene (CB) was spin coated to form active layers with 80 and 90 nm thick in first and second cell, respectively.

Characterizations: J–V characteristics of OSCs were measured by using Keithley 2635 source meter and ABET AM 1.5 G solar simulator with a light intensity of 100 mW cm^{-2}. The WF of different carrier transport layers were measured by SKP5050 Scanning Kelvin Probe System (KP Technology Ltd.). The ICL film thickness was measured by spectroscopic ellipsometry (J.A. Woollam Co. Inc.). The photoactive film thickness was measured by a Dektak alpha-step profile. To evaluate the total absorption of the device, the reflection of the device was measured, and the absorption of the devices was obtained by (100 −*R*)%. The reflection spectra were measured using a goniometer combined with a charge-coupled device (CCD) spectrometer and integrating sphere.

Supporting Information

Supporting Information is available from the Wiley Online Library or from the author.

Acknowledgements

S.L. and X.G. contributed equally to this work. H.L. provided help on low temperature J-V measurement. This study was supported by the University Grant Council of the University of Hong Kong (Grant Nos. 10401466 and 201111159062), the Collaborative Research Fund (Grant No. C7045-14E), the General Research Fund (Grant Nos. HKU711813 and HKU711612E), and ERG-SRFDP grant (M-HKU703/12) from the Research Grants Council of Hong Kong Special Administrative Region, China, and grant CAS14601 from CAS-Croucher Funding Scheme for Joint Laboratories. X.G. and F.H. thank the support by the Ministry of Science and Technology (Grant No. 2014CB643501), the Natural Science Foundation of China (Grant No. 21125419), Guangdong Natural Science Foundation (Grant No. S2012030006232), and Research Fund for the Doctoral Program of Higher Education of China (20120172140001).

Received: March 30, 2015
Revised: May 23, 2015
Published online: June 25, 2015

[1] a) K. M. Coakley, M. D. McGehee, *Chem. Mater.* **2004**, *16*, 4533; b) C. J. Brabec, N. S. Sariciftci, J. C. Hummelen, *Adv. Funct. Mater.* **2001**, *11*, 15; c) B. Kippelen, J.-L. Bredas, *Energy Environ. Sci.* **2009**, *2*, 251; d) C. J. Brabec, S. Gowrisanker, J. J. M. Halls, D. Laird, S. Jia, S. P. Williams, *Adv. Mater.* **2010**, *22*, 3839.

[2] a) X. Li, W. C. H. Choy, L. Huo, F. Xie, W. E. I. Sha, B. Ding, X. Guo, Y. Li, J. Hou, J. You, Y. Yang, *Adv. Mater.* **2012**, *24*, 3046; b) X. Li, W. C. H. Choy, H. Lu, W. E. I. Sha, A. H. P. Ho, *Adv. Funct. Mater.* **2013**, *23*, 2728; c) X. Yang, C.-C. Chueh, C.-Z. Li, H.-L. Yip, P. Yin, H. Chen, W.-C. Chen, A. K. Y. Jen, *Adv. Energy Mater.* **2013**, *3*, 666.

[3] a) J. Y. Kim, S. H. Kim, H. H. Lee, K. Lee, W. Ma, X. Gong, A. J. Heeger, *Adv. Mater.* **2006**, *18*, 572; b) J. Gilot, I. Barbu, M. M. Wienk, R. A. Janssen, *Appl. Phys. Lett.* **2007**, *91*, 113520.

[4] Y. Liu, J. Zhao, Z. Li, C. Mu, W. Ma, H. Hu, K. Jiang, H. Lin, H. Ade, H. Yan, *Nat. Commun.* **2014**, *5*, 5293.

[5] a) R. Steim, F. R. Kogler, C. J. Brabec, *J. Mater. Chem.* **2010**, *20*, 2499; b) V. Shrotriya, G. Li, Y. Yao, C.-W. Chu, Y. Yang, *Appl. Phys. Lett.* **2006**, *88*, 073508; c)Z. A. Tan, S. Li, F. Wang, D. Qian, J. Lin, J. Hou, Y. Li, *Sci. Rep.* **2014**, *4*, 4691. d)W. Zhao, L. Ye, S. Zhang, B. Fan, M. Sun, J. Hou, *Sci. Rep.* **2014**, *4*, 6570. e) K. Zhang, C. Zhong, S. Liu, C. Mu, Z. Li, H. Yan, F. Huang, Y. Cao, *ACS Appl. Mater. Interfaces* **2014**, *6*, 10429; f) S.-W. Liu, C.-C. Lee, C.-F. Lin, J.-C. Huang, C.-T. Chen, J.-H. Lee, *J. Mater. Chem.* **2010**, *20*, 7800.

[6] a) H. Zhou, L. Yang, W. You, *Macromolecules* **2012**, *45*, 607; b) Y. Y. Liang, Z. Xu, J. B. Xia, S. T. Tsai, Y. Wu, G. Li, C. Ray, L. P. Yu, *Adv. Mater.* **2010**, *22*, E135; c) X. Liu, Y. Sun, B. B. Y. Hsu, A. Lorbach, L. Qi, A. J. Heeger, G. C. Bazan, *J. Am. Chem. Soc.* **2014**, *136*, 5697; d) J.-H. Kim, S. A. Shin, J. B. Park, C. E. Song, W. S. Shin, H. Yang, Y. Li, D.-H. Hwang, *Macromolecules* **2014**, *47*, 1613; e) C. Cui, W.-Y. Wong, Y. Li, *Energy Environ. Sci.* **2014**, *7*, 2276; f)Y. Lin, L. Ma, Y. Li, Y. Liu, D. Zhu, X. Zhan, *Adv. Energy Mater.* **2014**, *4*, 1300626; g) Y. Lin, J. Wang, S. Dai, Y. Li, D. Zhu, X. Zhan, *Adv. Energy Mater.* **2014**, *4*, 1400420; h) C. Mu, P. Liu, W. Ma, K. Jiang, J. Zhao, K. Zhang, Z. Chen, Z. Wei, Y. Yi, J. Wang, S. Yang, F. Huang, A. Facchetti, H. Ade, H. Yan, *Adv. Mater.* **2014**, *26*, 7224; i) H.-Y. Chen, J. Golder, S.-C. Yeh, C.-W. Lin, C.-T. Chen, C.-T. Chen, *RSC Adv.* **2015**, *5*, 3381; j) H. Bai, P. Cheng, Y. Wang, L. Ma, Y. Li, D. Zhu, X. Zhan, *J. Mater. Chem. A* **2014**, *2*, 778; k) T. Y. Chu, J. Lu, S. Beaupré, Y. Zhang, J. R. Pouliot, J. Zhou, A. Najari, M. Leclerc, Y. Tao, *Adv. Funct. Mater.* **2012**, *22*, 2345; l) T.-Y. Chu, J. Lu, S. Beaupré, Y. Zhang, J.-R. Pouliot, S. Wakim, J. Zhou, M. Leclerc, Z. Li, J. Ding, *J. Am. Chem. Soc.* **2011**, *133*, 4250.

[7] a) J. You, L. Dou, Z. Hong, G. Li, Y. Yang, *Prog. Polym. Sci.* **2013**, *38*, 1909; b) J. Jo, J. R. Pouliot, D. Wynands, S. D. Collins, J. Y. Kim, T. L. Nguyen, H. Y. Woo, Y. Sun, M. Leclerc, A. J. Heeger, *Adv. Mater.* **2013**, *25*, 4783; c) S. Kouijzer, S. Esiner, C. H. Frijters, M. Turbiez, M. M. Wienk, R. A. Janssen, *Adv. Energy Mater.* **2012**, *2*, 945.

[8] a) G. Dennler, M. C. Scharber, T. Ameri, P. Denk, K. Forberich, C. Waldauf, C. J. Brabec, *Adv. Mater.* **2008**, *20*, 579; b) N. Li, D. Baran, K. Forberich, F. Machui, T. Ameri, M. Turbiez, M. Carrasco-Orozco, M. Drees, A. Facchetti, F. C. Krebs, C. J. Brabec, *Energy Environ. Sci.* **2013**, *6*, 3407.

[9] a) J. Yang, R. Zhu, Z. Hong, Y. He, A. Kumar, Y. Li, Y. Yang, *Adv. Mater.* **2011**, *23*, 3465; b) J. WonáShim, *Energy Environ. Sci.* **2012**, *5*, 9827; c) V. S. Gevaerts, A. Furlan, M. M. Wienk, M. Turbiez, R. A. Janssen, *Adv. Mater.* **2012**, *24*, 2130; d) J. You, L. Dou, K. Yoshimura, T. Kato, K. Ohya, T. Moriarty, K. Emery, C.-C. Chen, J. Gao, G. Li, *Nat. Commun.* **2013**, *4*, 1446; e) S. K. Hau, H.-L. Yip, K.-S. Chen, J. Zou, A. K.-Y. Jen, *Appl. Phys. Lett.* **2010**, *97*, 253307.

[10] a) A. Yakimov, S. R. Forrest, *Appl. Phys. Lett.* **2002**, *80*, 1667; b) S. Sista, Z. Hong, L.-M. Chen, Y. Yang, *Energy Environ. Sci.* **2011**, *4*, 1606; c) H.-S. Shim, J.-H. Chang, S.-J. Yoo, C.-I. Wu, J.-J. Kim, *J. Mater. Chem. A* **2014**, *2*, 5450; d) R. Timmreck, S. Olthof, K. Leo, M. K. Riede, *J. Appl. Phys.* **2010**, *108*, 033108.

[11] a) D. Zhang, W. C. Choy, F.-X. Xie, X. Li, *Org. Electron.* **2012**, *13*, 2042; b) F. Xie, S.-J. Cherng, S. Lu, Y.-H. Chang, W. E. I. Sha, S.-P. Feng, C.-M. Chen, W. C. H. Choy, *ACS Appl. Mater. Interfaces* **2014**, *6*, 5367.

[12] J. Gilot, I. Barbu, M. M. Wienk, R. A. J. Janssen, *Appl. Phys. Lett.* **2007**, *91*, 113520.

[13] Z. He, C. Zhong, S. Su, M. Xu, H. Wu, Y. Cao, *Nat. Photonics* **2012**, *6*, 591.

[14] Y. Zhou, C. Fuentes-Hernandez, J. Shim, J. Meyer, A. J. Giordano, H. Li, P. Winget, T. Papadopoulos, H. Cheun, J. Kim, *Science* **2012**, *336*, 327.

[15] a) C.-P. Chen, Y.-D. Chen, S.-C. Chuang, *Adv. Mater.* **2011**, *23*, 3859; b) F. Xie, W. C. H. Choy, C. Wang, X. Li, S. Zhang, J. Hou, *Adv. Mater.* **2013**, *25*, 2051; c) K. Zilberberg, S. Trost, H. Schmidt, T. Riedl, *Adv. Energy Mater.* **2011**, *1*, 377; d) X. Li, F. Xie, S. Zhang, J. Hou, W. C. H. Choy, *Adv. Funct. Mater.* **2014**, *24*, 7348.

[16] a) S. R. Hammond, J. Meyer, N. E. Widjonarko, P. F. Ndione, A. K. Sigdel, A. Garcia, A. Miedaner, M. T. Lloyd, A. Kahn, D. S. Ginley, J. J. Berry, D. C. Olson, *J. Mater. Chem.* **2012**, *22*, 3249; b) X. Li, W. C. H. Choy, F. Xie, S. Zhang, J. Hou, *J. Mater. Chem. A* **2013**, *1*, 6614; c) Y.-J. Lee, J. Yi, G. F. Gao, H. Koerner, K. Park, J. Wang, K. Luo, R. A. Vaia, J. W. P. Hsu, *Adv. Energy Mater.* **2012**, *2*, 1193; d) S. Murase, Y. Yang, *Adv. Mater.* **2012**, *24*, 2459.

[17] a) J. R. Manders, S. W. Tsang, M. J. Hartel, T. H. Lai, S. Chen, C. M. Amb, J. R. Reynolds, F. So, *Adv. Funct. Mater.* **2013**, *23*, 2993; b) A. Garcia, G. C. Welch, E. L. Ratcliff, D. S. Ginley, G. C. Bazan, D. C. Olson, *Adv. Mater.* **2012**, *24*, 5368; c) K. H. Kim, C. Takahashi, T. Okubo, Y. Abe, M. Kawamura, *Appl. Surf. Sci.* **2012**, *258*, 7809; d) Z. Huang, G. Natu, Z. Ji, M. He, M. Yu, Y. Wu, *J. Phys. Chem. C* **2012**, *116*, 26239.

[18] L. Groenendaal, F. Jonas, D. Freitag, H. Pielartzik, J. R. Reynolds, *Adv. Mater.* **2000**, *12*, 481.

[19] a) J. Y. Kim, K. Lee, N. E. Coates, D. Moses, T.-Q. Nguyen, M. Dante, A. J. Heeger, *Science* **2007**, *317*, 222; b) C.-Y. Chang, L. Zuo, H.-L. Yip, Y. Li, C.-Z. Li, C.-S. Hsu, Y.-J. Cheng, H. Chen, A. K. Y. Jen, *Adv. Funct. Mater.* **2013**, *23*, 5084; c) C.-Y. Chang, L. Zuo, H.-L. Yip, C.-Z. Li, Y. Li, C.-S. Hsu, Y.-J. Cheng, H. Chen, A. K. Y. Jen, *Adv. Energy Mater.* **2014**, *4*, n/a.

[20] a) N. Li, T. Stubhan, D. Baran, J. Min, H. Wang, T. Ameri, C. J. Brabec, *Adv. Energy Mater.* **2013**, *3*, 301; b) S. Sista, M. H. Park, Z. Hong, Y. Wu, J. Hou, W. L. Kwan, G. Li, Y. Yang, *Adv. Mater.* **2010**, *22*, 380.

[21] a) X. Guo, F. Liu, B. Meng, Z. Xie, L. Wang, *Org. Electron.* **2010**, *11*, 1230; b) C. H. Chou, W. L. Kwan, Z. Hong, L. M. Chen, Y. Yang, *Adv. Mater.* **2011**, *23*, 1282; c) S. Olthof, R. Timmreck, M. Riede, K. Leo, *Appl. Phys. Lett.* **2012**, *100*, 113302.

[22] G. V. Jensen, M. Bremholm, N. Lock, G. R. Deen, T. R. Jensen, B. B. Iversen, M. Niederberger, J. S. Pedersen, H. Birkedal, *Chem. Mater.* **2010**, *22*, 6044.

[23] X. Guan, K. Zhang, F. Huang, G. C. Bazan, Y. Cao, *Adv. Funct. Mater.* **2012**, *22*, 2846.

[24] a) S. Zhong, R. Wang, H. Ying Mao, Z. He, H. Wu, W. Chen, Y. Cao, *J. Appl. Phys.* **2013**, *114*, 113709; b) H. Kang, S. Hong, J. Lee, K. Lee, *Adv. Mater.* **2012**, *24*, 3005; c) M. Jin Tan, S. Zhong, R. Wang, Z. Zhang, V. Chellappan, W. Chen, *Appl. Phys. Lett.* **2013**, *103*, 063303.

[25] a) J. You, C. C. Chen, Z. Hong, K. Yoshimura, K. Ohya, R. Xu, S. Ye, J. Gao, G. Li, Y. Yang, *Adv. Mater.* **2013**, *25*, 3973; b) Y. Liu, C.-C. Chen, Z. Hong, J. Gao, Y. M. Yang, H. Zhou, L. Dou, G. Li, Y. Yang, *Sci. Rep.* **2013**, *3*, 3356.